Supporting Information

Facile synthesis of AuIr alloy nanoparticles and their enhanced oxygen evolution reaction performance under acidic and alkaline conditions

Xiaomei Xu[1], Cun Liu[2], Pengfei Jiang[2], Sang-Hyun Choi[3],*, Taekyung Yu[1,]*,

[1]Department of Chemical Engineering, Integrated Engineering Major, College of Engineering, Kyung Hee University, Yongin, 17104, Republic of Korea

[2] College of Chemistry and Chemical Engineering, Xinjiang Agricultural University, 311 East Nongda Road, Urumqi 830052, China

[3] School of Robotics and Automation Engineering, Dongyang Mirae University, Seoul, 08221, Republic of Korea

*Corresponding author
E-mail addresses: tkyu@khu.ac.kr (T. Yu); code911@dongyang.ac.kr (S.-H. Choi)

1. Electrochemical Characterization.

A three-electrode system was adopted in the electrochemical measurement conducted on an electrochemical workstation (CHI760E, Chenhua Shanghai) at room temperature. To prepare the working electrode, the catalyst (1.1 mg) was dispersed in the mixture solution containing ethanol (560 μL) and Nafion solution (40 μL, 5 wt%, Du Pont). Then, 3.4 μL of the solution was transferred onto a glassy carbon electrode (GCE) with a working area of 0.07 cm^2. Carbon rod and the saturated calomel electrode (SCE) served as the counter electrode and reference electrode, respectively. All electrodes were activated and stabilized by cyclic voltammetry before testing. To evaluate the OER activities, linear sweep voltammetry (LSV) was conducted in N_2-saturated 1 M KOH (or 0.5 M H_2SO_4) electrolyte at 25 °C with a scan rate of 5 $mV \cdot s^{-1}$ under 620 rpm without the iR compensation. The electrochemical impedance spectroscopy (EIS) tests were carried out in the frequency range between 100 kHz and 0.01 Hz at 1.6 V (vs. RHE). Long-term stability performance of the catalyst was measured in 40 mL of 1 M KOH (or 0.5 M H_2SO_4) electrolyte using chronopotentiometry measurement at a constant current density of 10 $mA \cdot cm^{-2}$. Potentials in this work were all referred to the reversible hydrogen electrode (RHE) through the Nernst equation as follows eq. (1):

$$E\ (vs\ RHE) = E\ (vs.\ Hg/HgO) + 0.099 + 0.0591 * pH \qquad (1)$$

The electrochemically active surface areas (ECSAs) were studied based on the electrochemical double-layer capacitance (C_{dl}) according to eq. (2). To obtain C_{dl}, cyclic voltammetry (CV) curves were collected at different scan rates (20, 40, 60, 80, and 100 $mV \cdot s^{-1}$) in a non-Faradaic potential window. By establishing the relationship between the difference between anodic and cathodic currents at 0.1 V (vs. RHE) and the scan rate, a linear trend was obtained. C_{dl} was equal to one-half of the slope of the fitting line.

$$C_{dl} = (\Delta j = (j_a - j_c))/2 \qquad (2)$$

Turnover Frequency (TOF) is a measure of catalytic activity. It refers to the number of times a catalytic site converts a substrate into a product per unit time[1]. It's a critical parameter for evaluating the efficiency of catalysts in chemical reactions[2].

$$TOF=I/4nF \qquad (3)$$

where I is the current density at a definite overpotential; F is the Faraday's constant (96,485 $C \cdot mol^{-1}$); and n, the number of moles of the electrochemical materials on the electrode. The factors 4 are based on the assumption that four electrons are necessary to form on oxygen molecules.

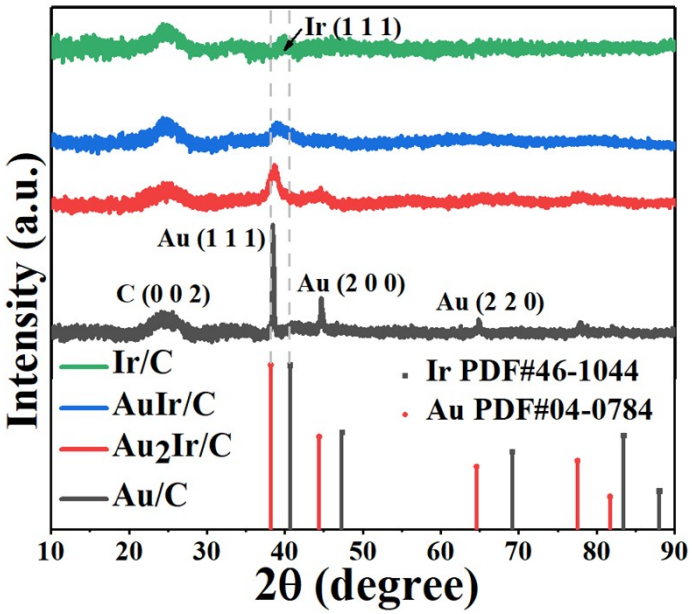

Fig. S1. (a) XRD patterns of the Au/C, Ir/C, AuIr/C and Au_2Ir/C NPs.

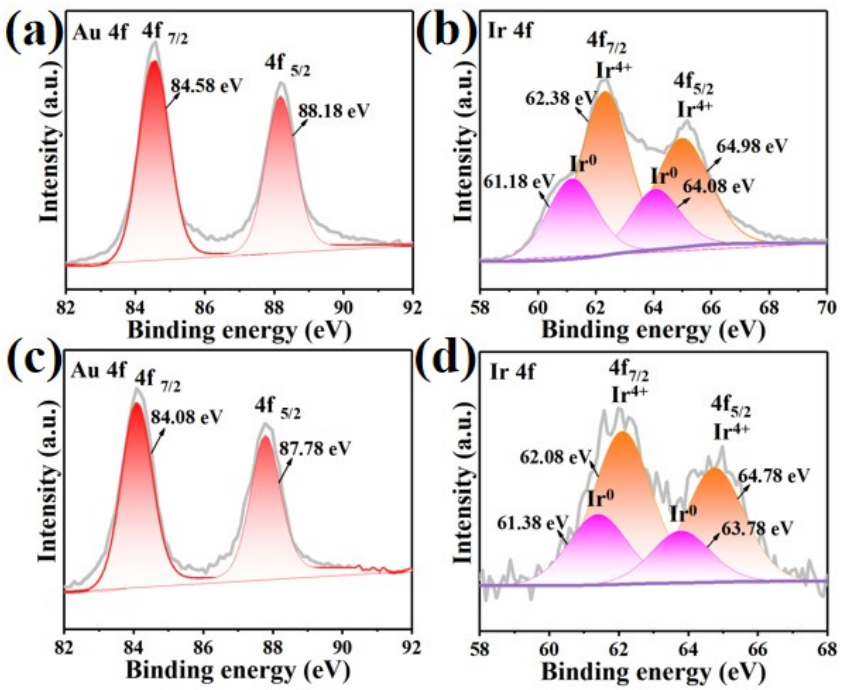

Fig. S2. (a) Au and (b) Ir 4f XPS spectra of the AuIr/C after OER test under alkaline conditions, respectively. (c) Au and (d) Ir 4f XPS spectra of the AuIr/C catalysts after OER test under acidic conditions, respectively.

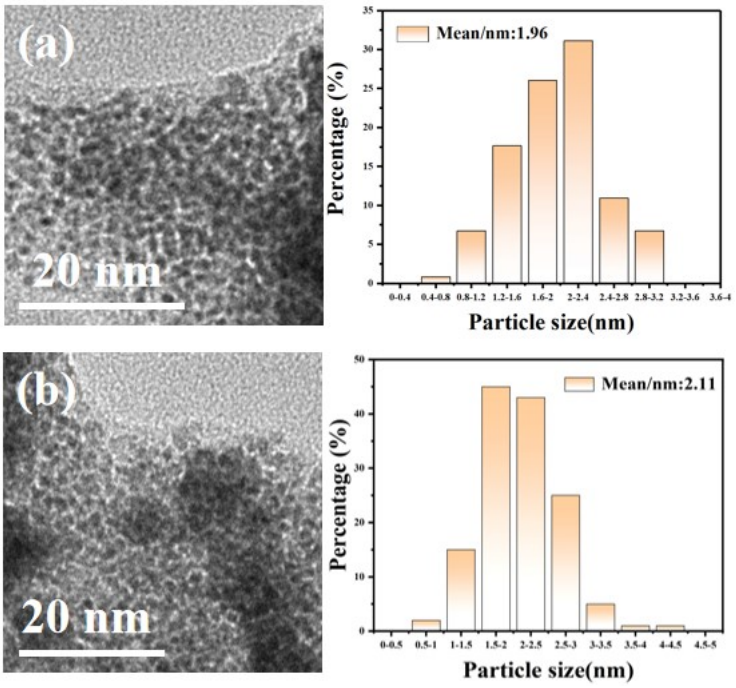

Fig. S3. TEM images and size distributions of (a) AuIr and (b) Au_2Ir alloy NPs.

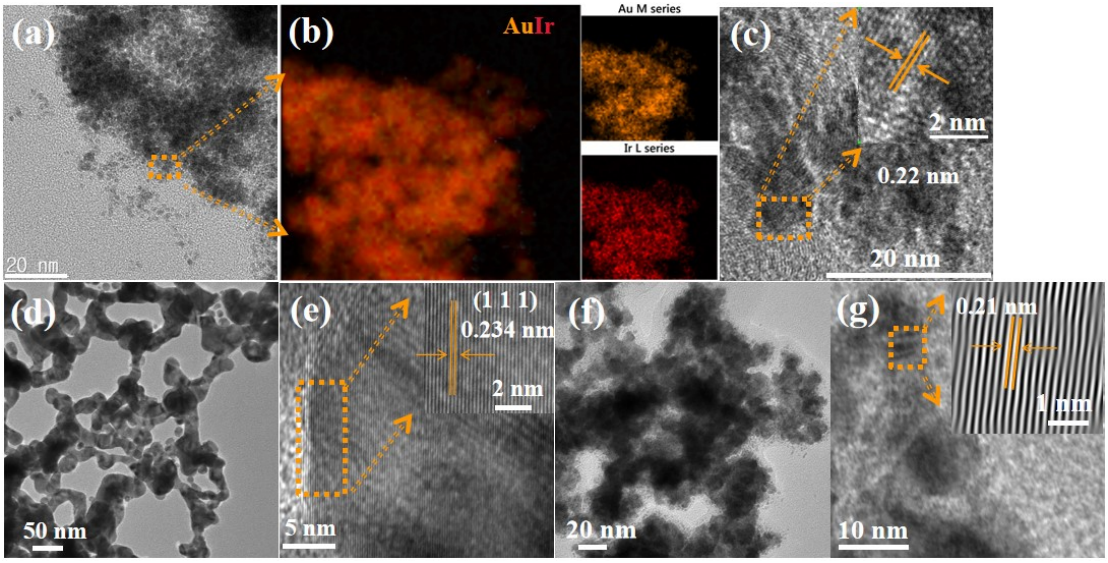

Fig. S4. (a) TEM, (b) EDS mapping and (c)HRTEM images of the AuIr alloy NPs. (d) TEM and (e) HRTEM images of the Au NPs. (f) TEM and (g) HRTEM images of the Ir NPs (inset is the fast Fourier transform (FFT) patterns).

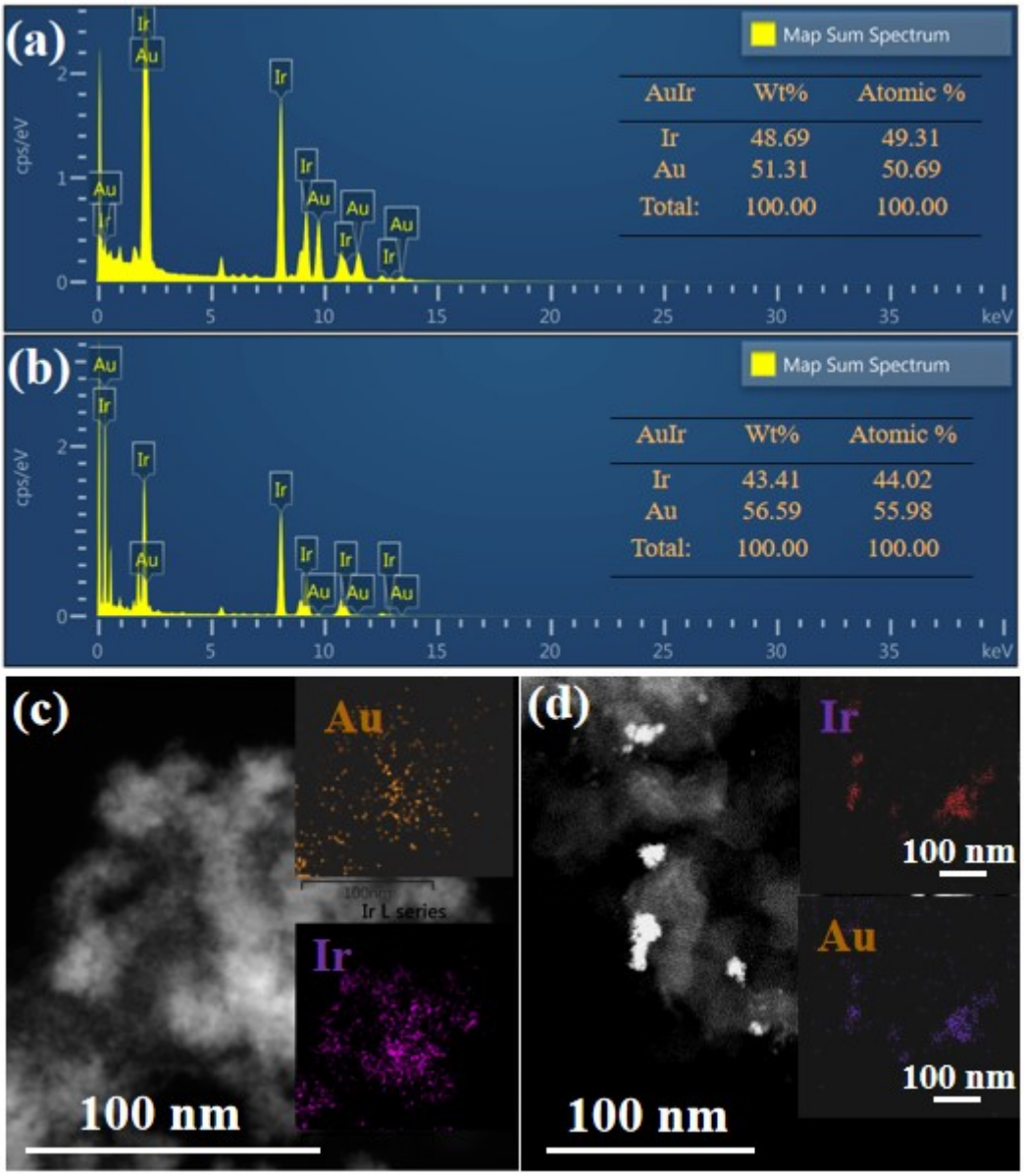

Fig. S5. Elemental compositions of the AuIr NPs (a) before and (b) after the OER test under alkaline conditions. EDS Mapping images of the AuIr catalysts after OER tests under (c) alkaline and (d) acidic conditions, respectively.

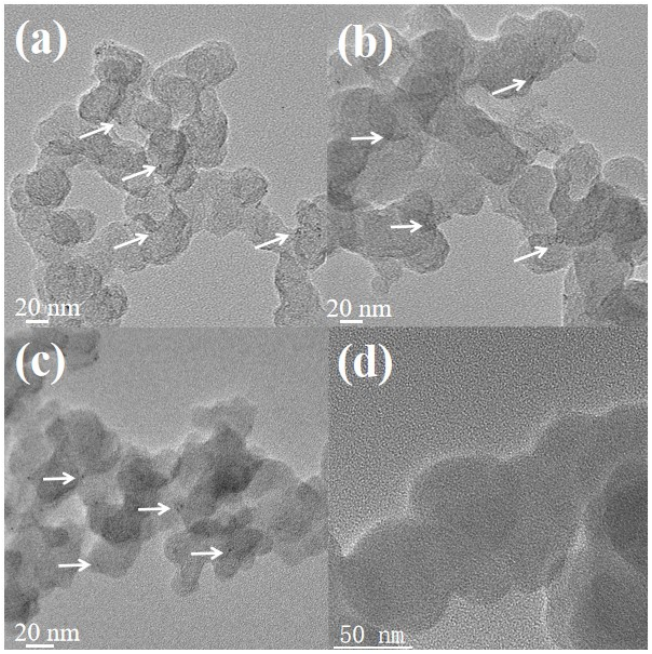

Fig. S6. TEM images of (a-b) AuIr/C, (c) Au_2Ir/C, and (d) Vulcan XC-72 carbon.

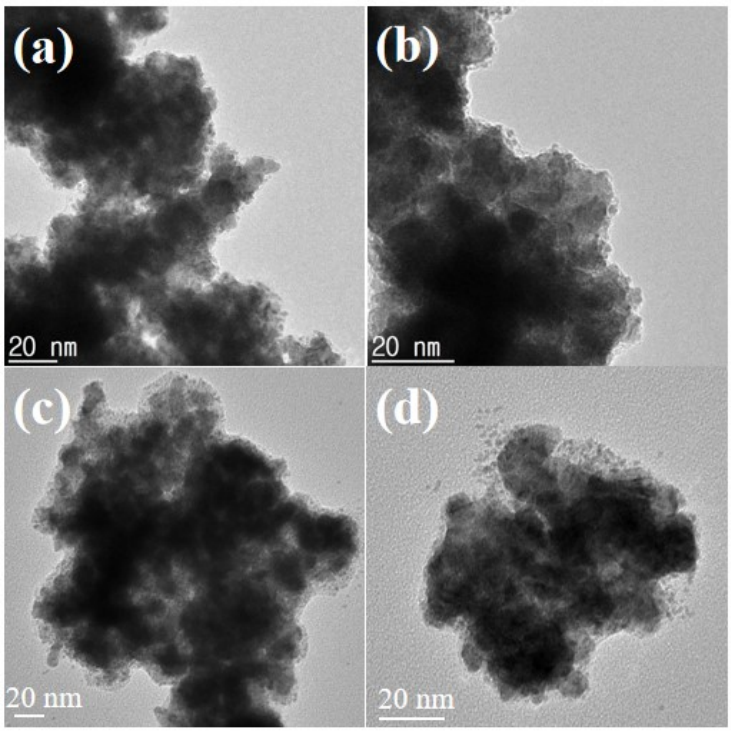

Fig. S7. TEM images of the AuIr/C catalysts after stability tests under (a and b) 1.0M KOH and (c and d) 0.5M H_2SO_4 conditions, respectively.

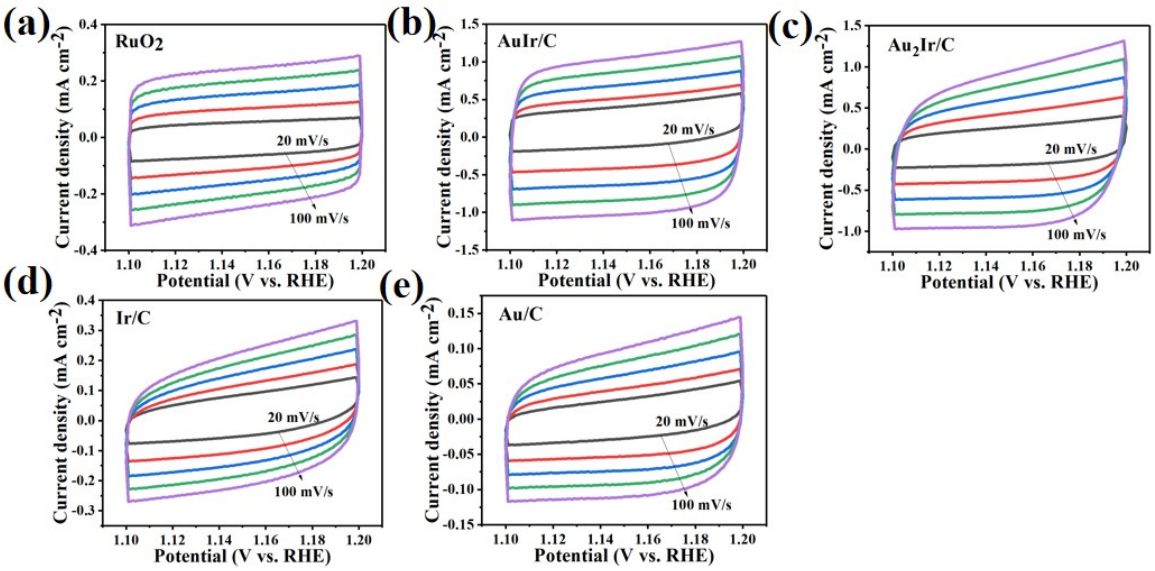

Fig. S8. CV curves of the (a) RuO_2, (b) AuIr/C, (c) Au_2Ir/C, (d) Ir/C, and (e) Au/C at different scan rates in 1.0 M KOH solution.

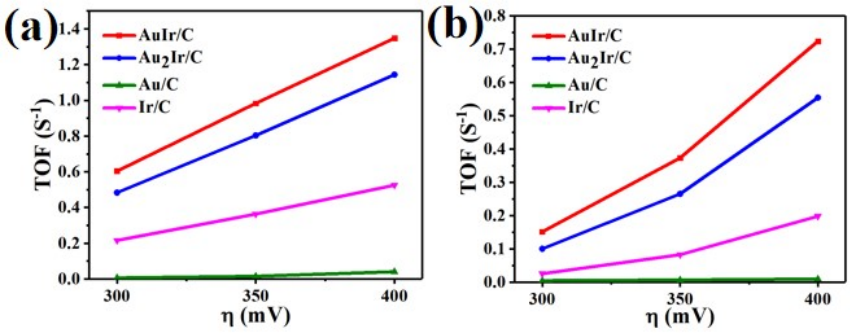

Fig. S9. TOFs calculated in (a) alkaline and (b) acidic solutions.

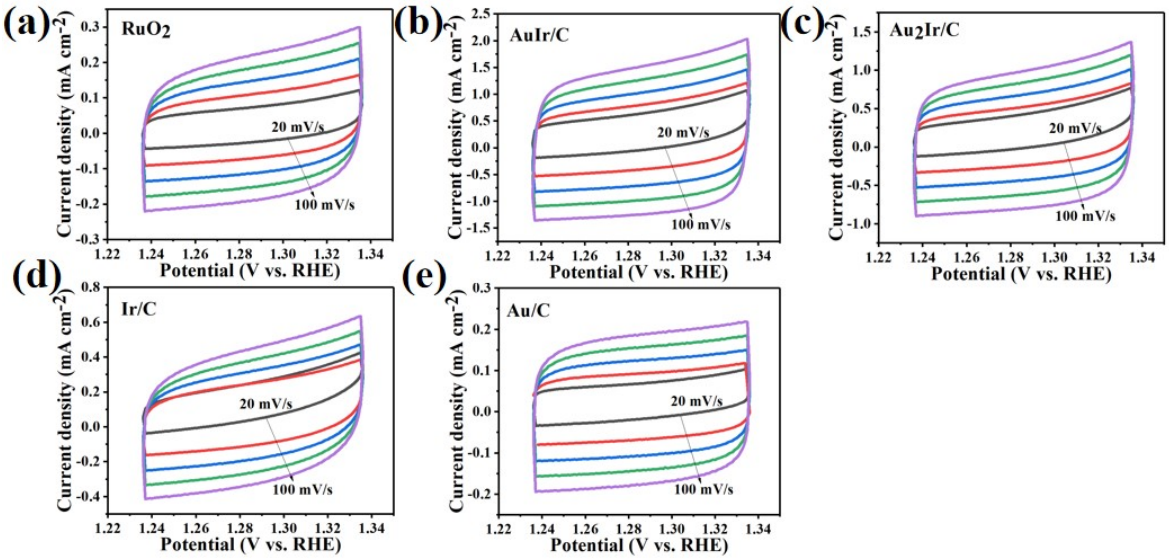

Fig. S10. (a-e) CV curves of the (a) RuO_2, (b) AuIr/C, (c) Au_2Ir/C, (d) Ir/C, and (e) Au/C at different scan rates in 0.5 M H_2SO_4 solution.

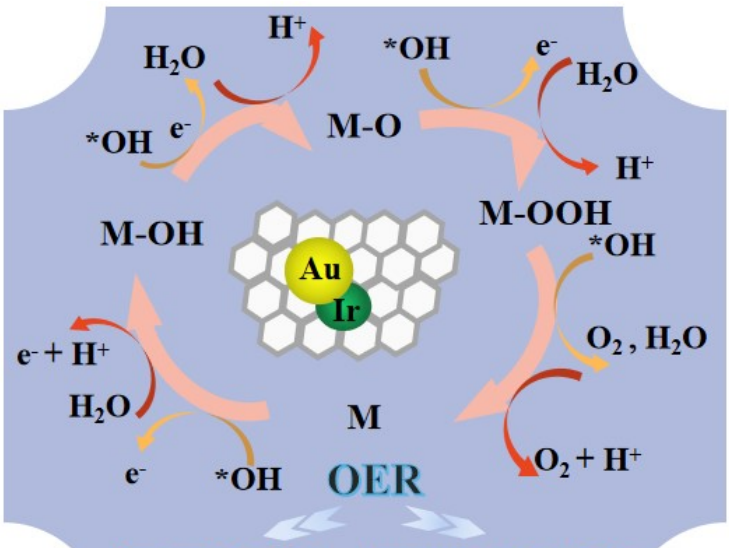

Fig. S11. The possible electrocatalytic mechanism of as-obtained AuIr/C for OER. The red and yellow lines indicate the reaction routes in acid and alkaline medium, respectively; the pink line explains the intermediate species (MOH, MO, MOOH) involved in the OER.

Table S1. Detailed information on the size, time, and temperature of synthesized AuIr NPs.

Sample	size (nm)	Temperature	Time	References
AuIr	1.96	80 ℃	3h	**This work**
Au_2Ir	2.11	80 ℃	3h	**This work**
$Au@AuIr_2$	7.94 ± 1.6	220 ℃	3h	[3]
Au_3Ir	5	250 °C	3h	[4]
AuIr	2.3-4.2	ice-water	4h	[5]
Au_5Ir_5	10	1.0 Pa (magnetron sputtering method)	-	[6]

Table S2. XPS data of the AuIr alloy NPs.

Samples	Binding Energy Au^0 4f 7/2 (eV)	Binding Energy Au^0 4f 5/2 (eV)	Binding Energy Ir^0 4f 7/2 (eV)	Binding Energy Ir^0 4f 5/2 (eV)	Binding Energy Ir^{4+} 4f 7/2 (eV)	Binding Energy Ir^{4+} 4f 5/2 (eV)
Au_2Ir	83.38	86.92	61.20	64.09	61.96	64.80
AuIr	83.63	87.23	60.89	63.96	62.41	64.82

Table S3. ICP data of the AuIr alloy NPs.

Samples	C_{Au}(mg/mL)	C_{Ir}（mg/mL)	Au/Ir Mole ration
AuIr	1.53	1.56	1.04:1
Au_2Ir	2.84	1.35	1.88:1

Table S4. Catalytic properties for OER of noble metal electrocatalysts in electrolyte.

Catalysts	electrolyte	OER η(mV)@j(mA/cm^2)	Tafel slope (mV·dec^{-1})	References
AuIr/C	**1.0 M KOH**	**230@10**	**59.0**	**This work**
	1.0 M KOH	**255@20**		
	1.0 M KOH	**344@50**		
AuIr/C	**0.5 M H_2SO_4**	**299@10**	**127.8**	**This work**
	0.5 M H_2SO_4	**330@20**		
	0.5 M H_2SO_4	**340@50**		
$RuCrFeCoNiO_x$	1.0 M KOH	239@10	62.7	[7]
Ir-$NiMoO_4$/Ir-Co_1Mn_1 LDH	1.0 M KOH	287@10	99.1	[8]
Ru-CoO	1.0 M KOH	340@10	84.1	[9]
IrNi/NiO HT	0.05 M H_2SO_4	329@10	64.0	[10]
Au-IrCo	0.1 M $HClO_4$	330@10	79.0	[11]
Ir-Pi	0.1 M phosphate	320@0.3	-	[12]
$IrCo_{13.3}O_{20.1}$	1.0 M KOH	152@10	60.5	[13]
Ir_2Cu	0.1 M $HClO_4$	349 @10	56.8	[14]
$Pt_{62}Co_{23}/Ir_{15}$ FBNWs/C	0.1 M $HClO_4$	308@10	-	[15]
$Ir_{0.30}Cu_{0.70}$	0.1 M $HClO_4$	292@10	100	[16]

Reference

1 . M.-G. Kim, H.J. Lee, T.K. Lee, E. Lee, H. Jin, J.-H. Park, S.Y. Cho, S. Lee, H.C. Ham, S.J. Yoo, *ACS Energy Lett.*, 2024, 2876-2884.

2 . B. Zhang, W. Li, K. Zhang, J. Gao, Y. Cao, Y. Cheng, D. Chen, Q. Wu, L. Ding, J. Tu, X. Zhang, C. Sun, *J. Mater. Sci. Technol.* , 2024, 214-223177.

3 . H. Wang, Z.-n. Chen, D. Wu, M. Cao, F. Sun, H. Zhang, H. You, W. Zhuang, R. Cao, *J. Am. Chem. Soc.*, 2021, 4639-4645143.

4 . Z.-X. Qian, C.-K. Peng, M.-F. Yue, L.-C. Hsu, J.-S. Zeng, D.-Y. Wei, Z.-Y. Du, G.-Y. Xu, H. Zhang, J.-H. Tian, S.-Y. Chen, Y.-G. Lin, J.-F. Li, *Small Methods*, 2023, 2301504.

5 . L. Yuan, Z. Yan, L. Jiang, E. Wang, S. Wang, G. Sun, *J. Energy Chem*., 2016, 805-81025.

6 . C. Zhai, R. Ming, H. Chen, L. Tan, N. Cong, J. Han, X. Zhou, X. Yang, Z. Ren, Y. Zhu, *Chem. Commun.*, 2020, 15028-1503156.

7 . W. Rong, Y. Chen, R. Dang, K. Huang, J. Xia, B. Zhang, J. Liu, H. Meng, Q. Cao, J. Wu, *J. Alloys Compd.*, 2024, 172786971.

8 . S. Tang, Y. Zhou, X. Lu, Z. Chen, Z. Huang, Z. Li, L. Tian, *J. Alloys Compd.*, 2022, 166415924.

9 . H.-W. Wu, Y. Cui, G.-H. Gao, Y.-J. Wang, J.-S. Li, *J. Alloys Compd*., 2023, 170847960.

10 . C. Spöri, P. Briois, H.N. Nong, T. Reier, A. Billard, S. Kühl, D. Teschner, P. Strasser, *ACS Catal*., 2019, 6653-66639.

11 . P.-C. Chen, M. Li, J. Jin, S. Yu, S. Chen, C. Chen, M. Salmeron, P. Yang, *ACS Mater. Lett.*, 2021, 1440-14473.

12 . A. Irshad, N. Munichandraiah, *ACS Appl. Mater. Interfaces*, 2015, 15765-157767.

13 . C. Cai, M. Wang, S. Han, Q. Wang, Q. Zhang, Y. Zhu, X. Yang, D. Wu, X. Zu, G.E. Sterbinsky, Z. Feng, M. Gu, *ACS Catal*., 2021, 123-13011.

14 . Q. Shi, C. Zhu, H. Zhong, D. Su, N. Li, M.H. Engelhard, H. Xia, Q. Zhang, S. Feng, S.P. Beckman, D. Du, Y. Lin, *ACS Energy Lett*., 2018, 2038-20443.

15 . Y. Sun, B. Huang, Y. Li, Y. Xing, M. Luo, N. Li, Z. Xia, Y. Qin, D. Su, L. Wang, S. Guo, *Chem. Mater.*, 2019, 8136-814431.

16 . L. Zhou, X. Liu, K. Wang, X. Zhao, H. Pu, T. Zhang, J. Jia, K. Dong, Y. Deng, *Energy & Fuels*, 2020, 9956-996234.